First-Principle Study of Structural, Elastic Anisotropic, and Thermodynamic Properties of $P\bar{4}m2$-BC_7

Quan Zhang[a], Qun Wei[b,*], Haiyan Yan[b], Zixia Zhang[a], Qingyang Fan[a], Xiaofei Jia[d], Junqin Zhang[a] and Dongyun Zhang[e]

[a]School of Microelectronics, Xidian University, Xi'an 710071, PR China

[b]School of Physics and Optoelectronic Engineering, Xidian University, Xi'an 710071, PR China

[c]College of Chemistry and Chemical Engineering, Baoji University of Arts and Sciences, Baoji 721013, PR China

[d] Department of Electronic and Information Engineering, Ankang University, Ankang 725000, PR China

[e]National Supercomputing Center in Shenzhen, Shenzhen 518055, PR China

(Received November 24, 2014; in final form January 2016)

The structural, elastic anisotropy and thermodynamic properties of the $P\bar{4}m2$-BC_7 are investigated using first-principles density functional calculations and the quasi-harmonic Debye model. The obtained structural parameters and elastic modulus are in consistency with the available theoretical data. Elastic constants calculations show that $P\bar{4}m2$-BC_7 is elastic anisotropic. The bulk modulus as well as other thermodynamic quantities of $P\bar{4}m2$-BC_7 (including the Grüneisen constant, heat capacity and thermal expansion) on temperatures and pressures have also been obtained.

DOI: 10.12693/APhysPolA.129.329

PACS/topics: 71.15.Mb, 65.40.De, 62.20.de

1. Introduction

Discovering more new superhard materials has become a very important part in materials science and technology because of their essential functions in fundamental science and technological applications. Diamond is the hardest material ever known [1], and it has been successfully used in electronics [2], optic [3], materials science, and surgery [4]. However, its usage is limited because it is easy to react with oxygen and ferrous metals. The compounds formed of light atoms (e.g., B, C, N, and O) have attracted great attention, because they usually possess superhard characters. Up to now, many such compounds have been synthesized. They are all found to have outstanding properties such as high elastic modulus and hardness. Recently, considerable efforts have been made to synthesize and predict possible new superhard materials in B–C system, such as BC_2, BC_3, BC_5, and BC_7 [5–12]. For example, diamond-like BC_3 phase has been synthesized from the graphite-like BC_3 phase at 2033 ± 241 K and 50 GPa [10]. The *Pmma* phase was suggested to be the best candidate structure for experimentally synthesized diamond-like BC_3 with the Vickers hardness of 64.8 GPa [11]. Recently, a new $P\bar{4}m2$-BC_7 phase is predicted [12] by applying particle swarm optimization algorithm [13]. It has been proved to be mechanically and dynamically stable. In the present work, we systematically investigate the structural and mechanical properties of $P\bar{4}m2$-BC_7, including the elastic constants and the elastic anisotropy. Also, the thermodynamic properties, such as heat capacity, thermal expansion, isothermal bulk modulus, the Grüneisen parameters, and the Debye temperature of $P\bar{4}m2$-BC_7 are investigated by the quasi-harmonic Debye model.

*corresponding author; e-mail: weiaqun@163.com

2. Computational method

Our electronic structure calculations are performed based on the plane-wave pseudopotential density functional theory (DFT) [14, 15] as implement in Cambridge Serial Total Energy Package (CASTEP) code [16]. We employ the Vanderbilt ultrasoft pseudopotentials to describe the electronic interactions in the calculations. The exchange correlation energy is described in the generalized gradient approximation (GGA) using the Perdew–Burke–Enzerhof (PBE) functional [17]. The structure is optimized with the Broyden–Fletcher–Goldfarb–Shanno (BFGS) method [18]. In our calculations, the electronic wave functions are extended in a plane-wave basis set with energy cutoff of 400 eV. The k mesh is taken as $16 \times 16 \times 6$. The self-consistent convergence of the total energy is 5×10^{-6} eV/atom, the maximum force on the atom is 0.01 eV/Å, the maximum ionic displacement within 5×10^{-4} Å and the maximum stress within 0.02 GPa.

3. Results and discussion

3.1. Structural properties

To obtain the lowest-energy geometry for this crystal, the structure was optimized with relaxation of both lattice parameters and atomic positions. The optimized structural parameters of $P\bar{4}m2$-BC_7 are listed in Table I. One can see that our results are in good agreement with previous calculated results [12]. The lattice constants ratios a/a_0, b/b_0, c/c_0 and V/V_0 of $P\bar{4}m2$-BC_7 (where

TABLE I

Lattice constants a, c (in Å), and cell volume per formula unit V_0 (in Å^3) for$P\bar{4}m2$-BC_7.

method	a	c	V
GGA*	2.5319	7.4465	47.7343
GGA**	2.5158	7.4497	55.9713

* this work, ** Ref [12]

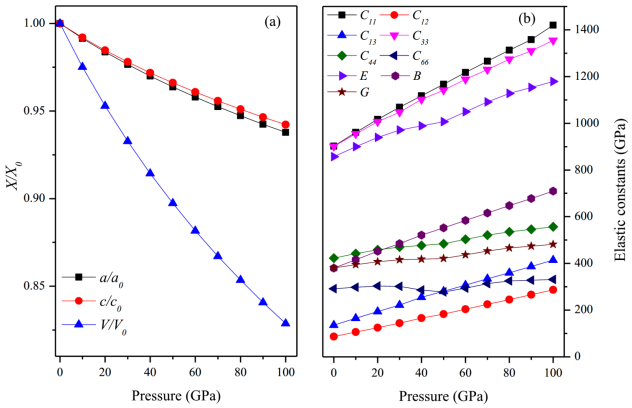

Fig. 1. (a) The lattice parameters a/a_0, and c/c_0 compression as functions of pressure for $P\bar{4}m2$-BC_7, and primitive cell volume V/V_0 for $P\bar{4}m2$-BC_7. (b) Elastic constants of $P\bar{4}m2$-BC_7 as a function of pressure.

a_0, b_0, c_0, and V_0 are the zero pressure equilibrium conventional lattice constants and volume, respectively) as a function of applied pressure are shown in Fig. 1a. All ratios decrease smoothly with pressure. It can be easily seen that the incompressibility along a-axis (b-axis) is less than that along c-axis. When the applied pressure increase from 0 GPa to 100 GPa, the volume V/V_0 changes from 1.0 to 0.83.

3.2. Elastic properties

The elastic constants play an important role for the determination of the mechanical properties and provide very important information about the nature of the interatomic forces. Particularly, they also provide information on the stability and stiffness of materials. In the present work, we calculated the elastic constants using the numerical first principles method. As known, there are six independent elastic constants (C_{11}, C_{33}, C_{44}, C_{66}, C_{12}, C_{13}, C_{16}) for tetragonal crystal. Results for the elastic constants are presented in Table II. The criteria for mechanical stability of $P\bar{4}m2$ symmetry is given by: $C_{11} > 0$, $C_{33} > 0$, $C_{44} > 0$, $C_{66} > 0$, $C_{11} - C_{12} > 0$, $C_{11} + C_{33} - 2C_{13} > 0$, and $2(C_{11} + C_{12}) + C_{33} + 4C_{13} > 0$ [19]. The elastic constants of the $P\bar{4}m2$ phase satisfy all the stability criteria, which indicates that the $P\bar{4}m2$-BC_7 is mechanically stable. The elastic constants versus pressure for $P\bar{4}m2$-BC_7 are displayed in Fig. 1b. As Fig. 1b shows, almost all the elastic constants C_{ij} increase with increasing pressure.

TABLE II

Calculated elastic constant C_{ij}, bulk modulus B, shear modulus G, the Young modulus E (all in [GPa]), the Poisson ratio of $P\bar{4}m2$-BC_7.

P	C_{11}	C_{12}	C_{13}	C_{33}	C_{44}	C_{66}	B	G	E	v	G/B
0	902	87	136	901	423	292	380	381	857	0.1243	1.00
0 [12]	939	26	154	852	491	326	377	421	920	0.0931	1.12
10	961	106	165	955	442	298	416	395	900	0.1394	0.95
20	1017	125	194	1007	458	303	452	407	939	0.1537	0.90
30	1069	144	222	1048	470	302	485	416	971	0.1665	0.86
40	1118	166	255	1102	477	286	521	418	989	0.1835	0.80
50	1167	183	281	1142	484	278	552	421	1007	0.196	0.76
60	1218	204	307	1188	503	294	584	437	1049	0.2005	0.75
70	1266	225	334	1230	521	313	616	453	1091	0.2047	0.74
80	1313	245	360	1274	535	325	648	466	1128	0.21	0.72
90	1358	266	387	1310	546	328	678	474	1153	0.2165	0.70
100	1402	287	414	1355	557	331	710	482	1179	0.2232	0.68

The bulk modulus B and shear modulus G are both measurements of the stiffness of an elastic material and always be used to characterize materials. B of a substance measures the substance resistance to uniform compression. G is concerned with the deformation of a solid when it experiences a force parallel to one of its surfaces while its opposite face experiences an opposing force (such as friction). A high (low) G/B value of a material shows its brittleness (ductility) manner. As is known empirically, the critical value, which separates ductility from brittleness, is about 0.57 [20]. If $G/B > 0.57$, a material behaves in a ductile manner, otherwise, a material represents brittleness. As Table II shows, our calculated value of G/B is 1.0 at 0 GPa, which indicates that $P\bar{4}m2$-BC_7 is brittle. With the pressure increasing to 100 GPa, the ratio decreased to 0.68, that is to say, $P\bar{4}m2$-BC_7 shows brittleness in the pressure range 0–100 GPa.

It is well known that the anisotropy of elasticity is an important implication in engineering science and crystal physics. So we go on investigating anisotropy of $P\bar{4}m2$-

BC_7. The Young modulus is defined as the ratio of normal stress to linear normal strain (both in the direction of applied load). The shear modulus is defined as the ratio of shear stress to linear shear strain. The Poisson ratio is defined as the ratio of transverse strain (normal to the applied load) to axial strain (in the direction of the applied load). The uniaxial stress can be represented as a unit vector, and advantageously described by two angles (θ, φ), we choose it to be the first unit vector in the new basis set a. The determination of some elastic properties (shear modulus, the Poisson ratio) requires another unit vector b, perpendicular to unit vector a and characterized by the angle χ. It is fully characterized by the angles θ, φ and χ. The coordinates of these vectors are: $a_1 = \sin\theta\cos\varphi$, $a_2 = \sin\theta\sin\varphi$, $a_3 = \cos\theta$, $b_1 = \cos\theta\cos\varphi\cos\chi - \sin\varphi\sin\chi$, $b_2 = \cos\theta\sin\varphi\cos\chi + \cos\varphi\sin\chi$, $b_3 = -\sin\theta\cos\chi$. The Young modulus and the Poisson ratio can be expressed as [21]:

$$E(\theta,\varphi) = \frac{1}{S'_{11}(\theta,\varphi)} = \frac{1}{N}, \tag{1}$$

and

$$v(\theta,\varphi,\chi) = -\frac{S'_{12}(\theta,\varphi,\chi)}{S'_{11}(\theta,\varphi)} = -\frac{M}{N}, \tag{2}$$

with

$$\begin{aligned} M = {} & a_1^2b_1^2S_{11} + a_2^2b_2^2S_{22} + \left(a_1^2b_2^2 + a_2^2b_1^2\right)S_{12} \\ & + \left(a_1^2b_3^2 + a_3^2b_1^2 + a_3^2b_2^2 + a_2^2b_3^2\right)S_{13} + a_3^2b_3^2S_{33} \\ & + \frac{1}{4}\left(4a_2a_3b_2b_3 + 4a_1a_3b_1b_3\right)S_{44} + a_1a_2b_1b_2S_{66}, \end{aligned} \tag{3}$$

and

$$\begin{aligned} N = {} & \left(a_1^4 + a_2^4\right)S_{11} + 2a_1^2a_2^2S_{12} + \left(2a_1^2a_3^2 + 2a_2^2a_3^2\right)S_{13} \\ & + a_3^4S_{33} + \frac{1}{4}\left(4a_2^2a_3^2 + 4a_1^2a_3^2\right)S_{44} \\ & + \tfrac{1}{4}\left(4a_1^2a_2^2\right)S_{66}. \end{aligned} \tag{4}$$

The shear modulus is obtained by applying a pure shear stress in the vector form and results in

$$\begin{aligned} 4G(\theta,\varphi,\chi)^{-1} = {} & \left(a_1^2b_1^2 + a_2^2b_2^2\right)S_{11} + 2a_1b_1a_2b_2S_{12} \\ & + \left(2a_1b_1a_3b_3 + 2a_2b_2a_3b_3\right)S_{13} + a_3^2b_3^2S_{33} \\ & + \tfrac{1}{4}\left(a_2^2b_3^2 + a_3^2b_2^2 + a_1^2b_3^2 + a_3^2b_1^2 + 2a_1b_3a_3b_1\right. \\ & \left. + 2a_2b_3a_3b_2\right)S_{44} + \tfrac{1}{4}\left(a_1^2b_2^2 + a_2^2b_1^2\right. \\ & \left. + 2a_1b_2a_2b_1\right)S_{66}. \end{aligned} \tag{5}$$

According to formulae above, we calculated The Young modulus, the Poisson ratio and shear modulus along different directions as well as the projections in different planes, as shown in Fig. 2. As Fig. 2a and b shows, the minimum of the Young modulus is 723 GPa and the maximum is 921 GPa, the average value of all directions is 863 GPa. The ratio $E_{\max}/E_{\min}$ =1.27 at 0 GPa and increase to 1.46 at 100 GPa, which shows that the anisotropy of the Young modulus increases with pressure. Figure 2c and d illustrate the 2D representation of the Poisson ratio in the xy and xz planes for $P\bar{4}m2$-BC_7. We obtained that $0 \le v \le 0.24$, showing that v remains positive at 0 GPa. When the pressure goes up from 0 GPa to 100 GPa, the minimal and maximal value of the Poisson ratio still keep positive. For the purpose to quantify the anisotropy, we obtained the maximal and minimal shear modulus for all directions of shear strain, the 2D representation of maximal and minimal shear modulus in the xy, xz, and yz planes for $P\bar{4}m2$-BC_7 are given in Fig. 2e and f. The shear modulus varies between 292 and 423 GPa, the ratio $G_{\max}/G_{\min} = 1.45$, the average value of all directions is 387 GPa. At 100 GPa, the ratio increases to 1.68.

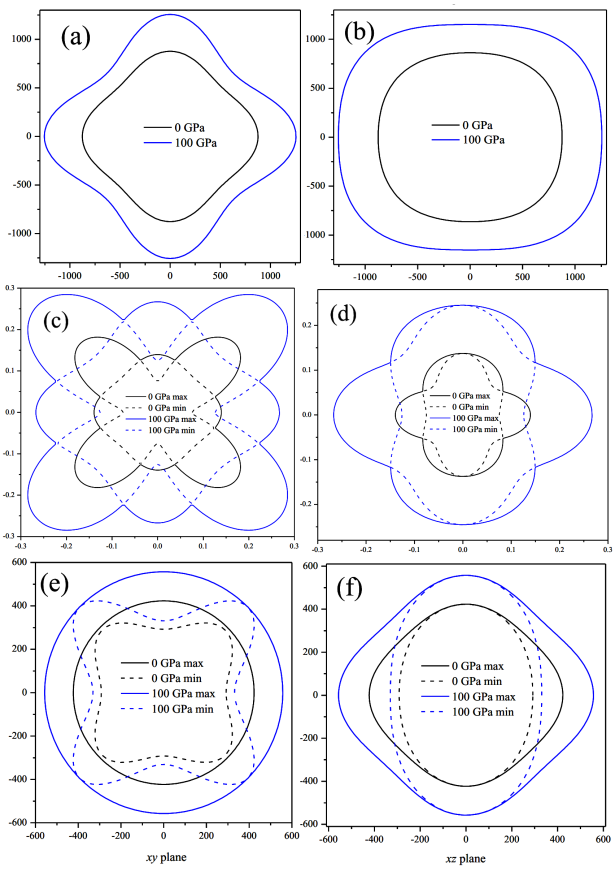

Fig. 2. 2D representation of the Young modulus (a)–(b), the Poisson ratio (c)–(d), and shear modulus (e)–(f) in the xy plane and xz plane.

The shear anisotropic factors provide a measurement of the degree of anisotropy in the bonding between atoms in different planes. The shear anisotropic factor for the {100} shear planes between the ⟨011⟩ and ⟨010⟩ directions is [22]:

$$A_1 = \frac{4C_{44}}{C_{11} + C_{33} - 2C_{13}}. \tag{6}$$

For the {100} shear plane between ⟨110⟩ and ⟨010⟩ directions it is [22]:

$$A_2 = \frac{2C_{66}}{C_{11} - C_{12}}. \quad (7)$$

For an isotropic crystal, the factors A_1 andA_2 must be 1.0, while any value smaller or greater than 1.0 is a measurement of the degree of elastic anisotropy. The calculated value of A_1 and A_2 is 1.11 and 0.72 at ambient pressure, respectively. From all calculated anisotropic parameters, it is concluded that the $P\bar{4}m2$-BC_7 compounds show elastic anisotropy.

3.3. Thermodynamic properties

To investigate the thermodynamic properties of $P\bar{4}m2$-BC_7, we use the quasi-harmonic Debye model which has been described in detail in Refs. [23–27]. The thermodynamic properties of $P\bar{4}m2$-BC_7 are determined in the temperature range from 0 K to 2000 K, meanwhile, the pressure effect is studied in the range 0–100 GPa. The calculated relationships of the Debye temperature on pressure and temperature are plotted in Fig. 3. One can see that the Debye temperature decreases with temperature at certain pressure. The lower the pressure is, the faster the Debye temperature decreases. The Debye temperature increases monotonously at given pressure.

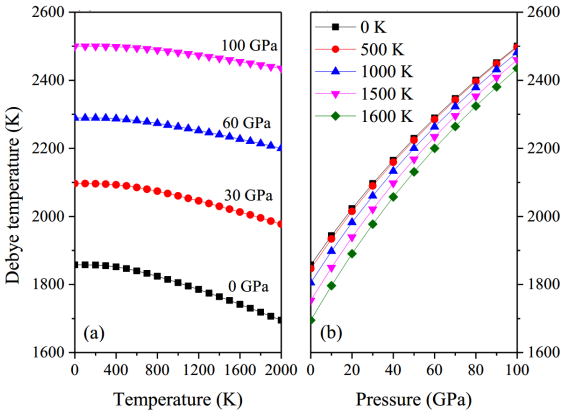

Fig. 3. Temperature (a) and pressure (b) dependence of the Debye temperature for $P\bar{4}m2$-BC_7.

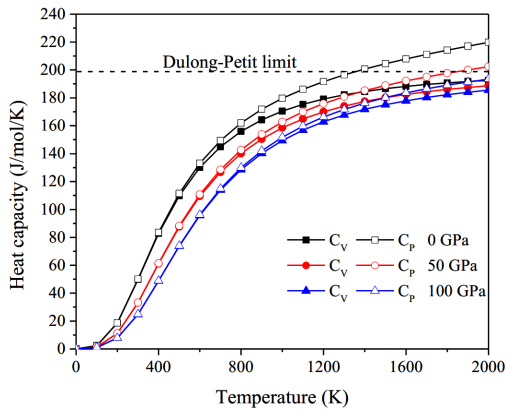

Fig. 4. Temperature dependence of the heat capacity at different pressures for $P\bar{4}m2$-BC_7.

The calculated relationships of heat capacity C_v and C_p at 0, 50, and 100 GPa on temperature are shown in Fig. 4. It can be seen that, at low temperature ($T < 300$ K), the difference between C_v and C_p is slight. At high temperature, C_v approaches a constant value, C_p increases monotonously with increments of the temperature. The anharmonic effect on C_v is suppressed at high temperatures, and C_v approaches a constant value called as the Dulong–Petit limit and C_p still increases monotonously with increments of the temperature. One can also see that both C_p and C_v increase with pressures at given temperature. The influences of the temperature on the heat capacity are much more significant than that of the pressure on them.

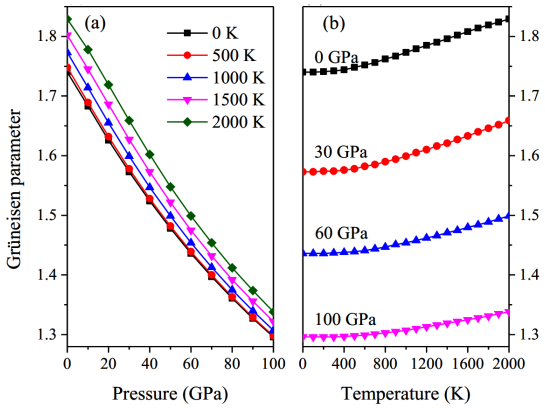

Fig. 5. Pressure (a) and temperature (b) dependence of the Grüneisen parameter for $P\bar{4}m2$-BC_7.

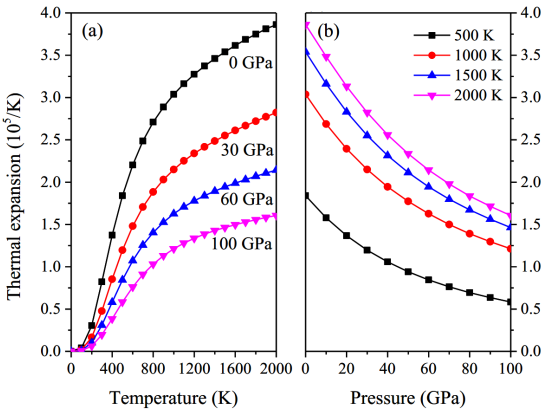

Fig. 6. Temperature (a) and pressure (b) dependence of the thermal expansion coefficient for $P\bar{4}m2$-BC_7.

In Fig. 5, we have plotted the Grüneisen parameter of $P\bar{4}m2$-BC_7 at various pressures and temperatures. It can be seen that the Grüneisen parameter decreases monotonously with pressure at given temperature. At given pressure, the Grüneisen parameter increases with temperature. At low temperature ($T < 400$ K), when the pressure keeps constant, the Grüneisen parameter almost keeps constant. At high temperature ($T > 400$ K),

the Grüneisen parameter increases linearly with temperature. From Fig. 5, we can find that the Grüneisen parameter variation is more sensitive to pressure than to temperature.

The pressures and temperatures' dependences of the thermal expansion coefficient α for the $P\bar{4}m2$-BC_7 are shown in Fig. 6. It can be seen from Fig. 6a that α increases faster at low temperatures than at high temperatures. At certain temperature, with the pressure increases, the thermal expansion coefficient decreases.

4. Conclusion

We have performed systematic first principles calculations to identify the structural properties of $P\bar{4}m2$-BC_7 which was recently proposed to be superhard. In this paper, we investigated the elastic anisotropic, electronic properties, and thermodynamic properties of $P\bar{4}m2$-BC_7. From the elastic stability criteria, we have proved this material to be stable up to 100 GPa. The B/G ratio indicates that $P\bar{4}m2$-BC_7 becomes more ductile in the pressure range of 0–100 GPa. Its elastic anisotropy increases with increasing pressure. Using the quasi-harmonic Debye model, the thermodynamic properties including the Debye temperature, the Grüneisen parameter, the heat capacity, and the thermal expansion coefficients of $P\bar{4}m2$-BC_7 are predicted under high temperature and high pressure.

Acknowledgments

This work was supported by the Fundamental Research Funds for the Central Universities, the National Natural Science Foundation of China (grant Nos. 11204007, 61474089), and the Scientific Research Fund of Shaanxi Provincial Education Department (grant No. 15JK1005)

References

[1] S. Veprek, *J. Vac. Sci. Technol. A* **17**, 2401 (1999).

[2] *Properties, Growth and Application of Diamond*, Eds. M.H. Nazaré, A.J. Neves, INSPEC, London 2001.

[3] A. Zaitsev, *Optical Properties of Diamond: A Data Handbook*, Springer, Berlin Heidelberg 2001.

[4] E.G. Harlow, *The Nature of Diamond*, Cambridge Univ. Press, New York 1998.

[5] V.L. Solozhenko, O.O. Kurakevych, D. Andrault, Y. Le Godec, M. Mezouar, *Phys. Rev. Lett.* **102**, 015506 (2009).

[6] Z. Liu, J. Yang, X. Guo, H. Sun, H.T. Wang, E. Wu, Y. Tian, *Phys. Rev. B* **73**, 172101 (2006).

[7] P.V. Zinin, L.C. Ming, H.A. Ishii, R. Jia, T. Acosta, *J. Appl. Phys.* **111**, 114905 (2012).

[8] J.E. Lowther, *J. Phys. Condens. Matter* **17**, 3221 (2005).

[9] K.M. Krishnan, *Appl. Phys. Lett.* **58**, 1857 (1991).

[10] P.V. Zinin, L.C. Ming, I. Kudryashov, N. Konishi, S.K. Sharma, *J. Raman Spectrosc.* **38**, 1362 (2007).

[11] H. Liu, Q. Li, L. Zhu, Y. Ma, *Phys. Lett. A* **375**, 771 (2011).

[12] H. Liu, Q. Li, L. Zhu, Y. Ma, *Solid State Commun.* **151**, 716 (2011).

[13] Y. Wang, J. Lv, L. Zhu, Y. Ma, *Phys. Rev. B* **82**, 094116 (2010).

[14] P. Hohenberg, W. Kohn, *Phys. Rev.* **136**, B864 (1964).

[15] W. Kohn, L.J. Sham, *Phys. Rev.* **140**, A1133 (1965).

[16] V. Milman, B. Winkler, J.A. White, C.J. Packard, M.C. Payne, E.V. Akhmatskaya, R.H. Nobes, *Int. J. Quant. Chem.* **77**, 895 (2000).

[17] J.P. Perdew, K. Burke, M. Ernzerhof, *Phys. Rev. Lett.* **77**, 3865 (1996).

[18] B.G. Pfrommer, M. Cote, S.G. Louie, M.L. Cohen, *J. Comput. Phys.* **131**, 233 (1997).

[19] Z.J. Wu, E.J. Zhao, H.P. Xiang, X.F. Hao, X.J. Liu, *Phys. Rev. B* **76**, 054115 (2007).

[20] S.F. Pugh, *Philos. Mag.* **45**, 823 (1954).

[21] A. Marmier, Z.A.D. Lethbridge, R.I. Walton, C.W. Smith, S.C. Parker, K.E. Evans, *Comput. Phys. Commun.* **181**, 2102 (2010).

[22] D. Connétable, O. Thomas, *Phys. Rev. B* **79**, 094101 (2009).

[23] M.A. Blanco, E. Francisco, V. Luaña, *Comput. Phys. Commun.* **158**, 57 (2004).

[24] M. Zhang, H. Yan, Q. Wei, D. Huang, *Trans. Nonferrous Met. Soc. China* **23**, 3714 (2013).

[25] M.A. Blanco, A. Martín Pendás, E. Francisco, J.M. Recio, R. Franco, *J. Mol. Struct. Theochem.* **368**, 245 (1996).

[26] H. Yan, M. Zhang, D. Huang, Q. Wei, *Solid State Sci.* **18**, 17 (2013).

[27] E. Francisco, M.A. Blanco, G. Sanjurjo, *Phys. Rev. B* **63**, 094107 (2001).